Desalination and Water Treatment
www.deswater.com

doi:10.5004/dwt.2019.24383

164 (2019) 339–345
October

Efficiency of zinc stannate/multi-walled carbon nanotubes as the nanocomposite photocatalyst in the removal of methylene blue from aqueous solutions

Hossein Karimi[a,b], Samira Taherkhani[c,*], Hamidreza Pourzamani[b], Nasrin Fathi[a], Mahsa Khajeh[a]

[a]*Student Research Committee, Isfahan University of Medical Sciences, Isfahan, Iran, email: h.karimi.m90@gmail.com (H. Karimi), fathi_nasrin@yahoo.com (N. Fathi), khajeh.mahsa22@gmail.com (M. Khajeh)*
[b]*Department of Environmental Health Engineering, School of Public Health, Isfahan University of Medical Sciences, Isfahan, Iran, email: pourzamani@hlth.mui.ac.ir (H. Pourzamani)*
[c]*Department of Chemistry, Faculty of Science, University of Zanjan, Zanjan, Iran, Tel. +98 9141240128, email: taherkhani_s@ymail.com (S. Taherkhani)*

Received 8 January 2019; Accepted 9 May 2019

ABSTRACT

In the present study, the use of synthesized zinc stannate/multi-walled carbon nanotubes (ZSC) nanocomposite was investigated as the photocatalyst in the removal of methylene blue (MB) under visible light. The ZSC nanocomposite was synthesized by the hydrothermal method. The structural properties of the synthesized nanocomposite were investigated by X-ray diffraction (XRD), Fourier-transform infrared spectroscopy (FT-IR), scanning electron microscopy (SEM), and UV-visible diffuse reflectance spectroscopy (DRS). The optimal values of parameters for the removal of the dye were as follows: 130 mg·L^{-1}photocatalyst dosage, 10 mg·L^{-1}dye concentration, pH = 9, and 10 cm distance of radiation source. In this condition, the removal degree was 94%. The photocatalytic removal of dye was followed by pseudo-first-order kinetic and Langmuir-Hinshelwood kinetic models. Furthermore, the values of the equilibrium constant of adsorption (K_{ads})and the rate constant of the surface reaction (k_c) were obtained as 0.91 L·mg^{-1} and 0.84 mg·L^{-1}·min^{-1}, respectively.

Keywords: Photocatalyst; Dye removal; Zn_2SnO_4; MWCNTs; Nanocomposite

1. Introduction

The textile industry is one of the most expansive industries in the world, considerably grown due to the increasing global demand for its products and the growth of related industries [1–4]. If the effluent of this industry which has low doses of dye substances is released into the environment, the receiving waters will be harmful to plants and algae and, consequently, to human health [5–8]. Also, some of the dyes and their byproducts generated from decomposition are aromatic compounds that are highly carcinogenic and resistant to the biodegradation process [9–11]. The methylene blue (MB) used as the target pollutant in this research is an aquatic cationic dye, widely incorporated in textile and plastic industries. Finding an effective process for the removal of dye contaminants from sewage has led to various research efforts.

In recent decades, several methods have been investigated for the removal of dyes,such as advanced oxidation processes (AOPs) [12–14]. The use of photocatalyst as an AOP is a practical and effective process in wastewater treatment. The semiconductor acts as a photocatalyst in the presence of light sources, leading to the removal of contaminating agents. In previous studies, binary oxides (ZnO, TiO_2, etc.) with carbon nanotubes have been employed as photocatalyst in the removal of organic pollutants [15–17]. Zinc stannate (ZS) is a triodesemiconductor oxide with unique optical and electrical properties due to characteristics such as stability at all pH levels. It is used as a photocatalyst in the removal of organic materials such as dyes. Moreover, it has a physical and chemical ability to combine with carbon nano-

*Corresponding author.

tubes [18]. ZS, as one of the most important ternary oxides, has been studied in a wide range of applications such as an anode material for dye-sensitized solar cells (DSCs) [19], Li^+ batteries [20], and photocatalysts for pollution decomposition. Increasing the photocatalytic activity of semiconductors along with carbon nanotubes can be justified by various mechanisms. The use of carbon nanotubes in the structure of nanocomposites has been highly regarded for their unique thermal, electrical, and mechanical properties. The wide cross-section, high porosity, and laminate structure increase the efficiency of this material to absorb all types of contaminants. In fact, the presence of carbon nanotubes leads to the transfer of a photoexcited electron from the photocatalyst valence band to the carbon nanotube conduction band. According to the position of the energy levels, the energy required for this transfer may have wavelengths close to the visible light range [21,22]. In the present study, the application of the synthesized zinc stannate/multi-walled carbon nanotubes (ZSC) nanocomposite was investigated as a photocatalytic in the removal of MB under visible light, and the kinetics of photocatalytic reaction was determined.

2. Materials and methods

Multi-walled carbon nanotubes (MWCNTs, 20 nm in diameter and 30 μm in length, purity > 95 wt%) was purchased from Neutrino Co. (Iran). Stannic chloride pentahydrate ($SnCl_4{\cdot}5H_2O$), zinc nitrate, and MB as the target pollutant were purchased from Boyakhsaz Co. (Iran) and NaOH was purchased from Merck (Germany). Deionized distilled water was used in all the experiments, and all the experiments were repeated in triplicate.

The equipment used in this study included: a digital pH meter (Metrohm 780/Swiss) for adjusting the pH of the solution, a UV-Vis spectrophotometer (Shimadzu UV-160/Japan), a magnetic stirrer (HelidolphMr 3001, k/Germany), an ultrasonic bath (CD-4820), an autoclave, digital oven (Pars Azma, Iran), and an electronic furnace (SybornThermolyne, 1500 Furnace).

3. Characterization

The structure, phase composition, and real size of the prepared nanocomposites were determined by Powder XRD examination using Siemens X-ray diffraction ((D5000, Germany) with Cu K-alpha radiation(1.54065 Å and θ = 5–75)). The surface morphology of nanocomposites was verified by field-emission scanning electron microscopy (FESEM, MIRA3 FEG-SEM,TESCAN).

3.1. Synthesis of ZSC

In order to synthesize ZSC nanocomposite, first 0.05 g of MWCNTs was dispersed into deionized water by sonication for 15 min. Then, $SnCl_4{\cdot}5H_2O$ (3 mg) and $Zn(NO_3)_2$ (3 mg) were dissolved in 20 mL of double distilled water separately to give two transparent solutions. Afterward, 20 mL of NaOH (1 M) was added dropwise to the tin chloride dihydrate solution, and the resulting solution was added drop by drop to the MWCNT solution. After that, under vigorous stirring at room temperature, the zinc nitrate solution was added to the previous mixed solution until the formation of a gray precipitate of the hybrid complex. Finally, the gray precipitate was transferred to a 100 mL stainless Teflon-lined. The autoclave was sealed and maintained in a furnace at 220°C for 48 h. The autoclave was cooled naturally to room temperature. The resulting precipitate was washed several times with double distilled water and absolute ethanol by repeated centrifugation and ultrasonication. Finally, the product was dried in an oven at 80°C for 20 h.

3.2. Photocatalytic degradation efficiency of the synthesized nanocomposites

The photocatalytic activity of the synthesized nanocomposite was investigated by the degradation of MB under visible light (power = 26 W). All experiments were conducted in a 200 mL beaker as the batch reactor with a magnetic stirrer. Sampling was performed at intervals of 0–90 min and absorbance was determined using the UV-Vis-spectrophotometer at 668 nm (Shimadzu UV-160/Japan) in order to measure dye concentration. The removal efficiency was calculated using the following equation:

$$Dye\ removal\% = \frac{C_0 - C_t}{C_0} \times 100 \quad (1)$$

where C_0 and C_t are the initial concentration and concentration of dye at time t, respectively.

4. Results and discussion

4.1. Characterization of the hydrothermally synthesized nanocomposite

Fig. 1 illustrates the Fourier-transform infrared spectroscopy (FT-IR) spectra of ZS and hydrothermally synthesized ZSC. In the spectrum of zinc oxide (Fig. 1b), two absorption peaks observed in 520 and 682 cm^{-1} were related to the tensile vibrations of ZnO and SnO, respectively. Two small absorption peaks in 1039 and 2917 cm^{-1} belonged to symmetric and asymmetric tensile vibrations of Zn-O-Sn, respectively. In addition, the absorption peak at 3444 cm^{-1} was related to the tensile vibrations of –OH at the ZS surface. Compared to pure ZS, the peak intensity of ZSC was lower. The presence

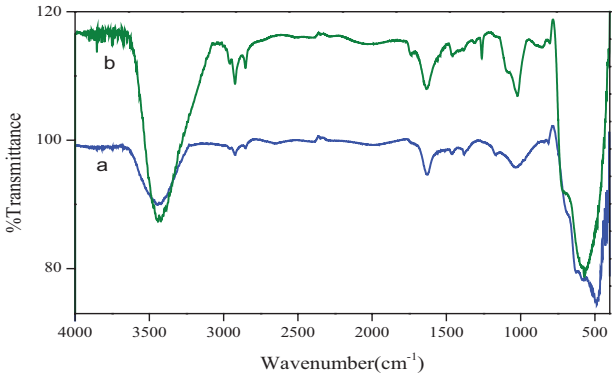

Fig. 1. FT-IR spectra of ZSC (a) and ZS (b).

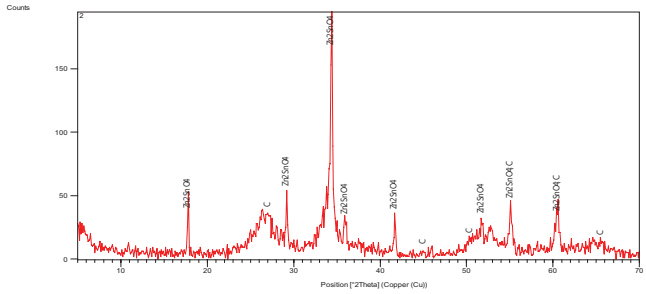

Fig. 2. XRD pattern spectrum of the prepared ZSC.

of carbon nanotubes reduced the mass/volume percentage of metal oxide in the nanocomposite and weakened the absorption peaks of ZS. A slight displacement of the absorption peaks of nanocomposite ZSC compared with pure ZS can be explained on the basis of the formation of interactions between carbon nanotubes and ZS particles [23,24].

In order to confirm the results of FT-IR, X-ray diffraction (XRD) analysis was performed on both pure ZS and ZSC (Fig. 2). The data were in good agreement with the Joint Committee of Powder Diffraction Standards (JCPDS) card number [01-073-1725] (for the structure of ZS) [19,25].

The morphology of the prepared ZSC was also characterized by the scanning electron microscopy (SEM) technique (followed by Au coated by the sputtering method using a coater sputter SC 761). Fig. 3 depicts the SEM image of the prepared ZSC. The carbon nanotubes in the ZS matrix are observed in the form of nanorods (<60 nm).

Fig. 4 shows the diffuse reflectance spectra (DRS) of ZS and ZSC. It is well known that DRS can be used to examine the optical absorption properties of photocatalysts. The UV-vis absorption spectrum revealed that ZS absorbed only short wavelengths <340 nm, which is attributed to its inartistic band gap. In the ZS UV-vis spectrum, it is clear that adding MWCNTS to ZS resulted in a change in the absorption edge at longer wavelengths (400 nm). The optical band gap energies for the prepared photocatalysts were determined by Tauc-Mott plot (TM) derived from the following equation [18,26]:

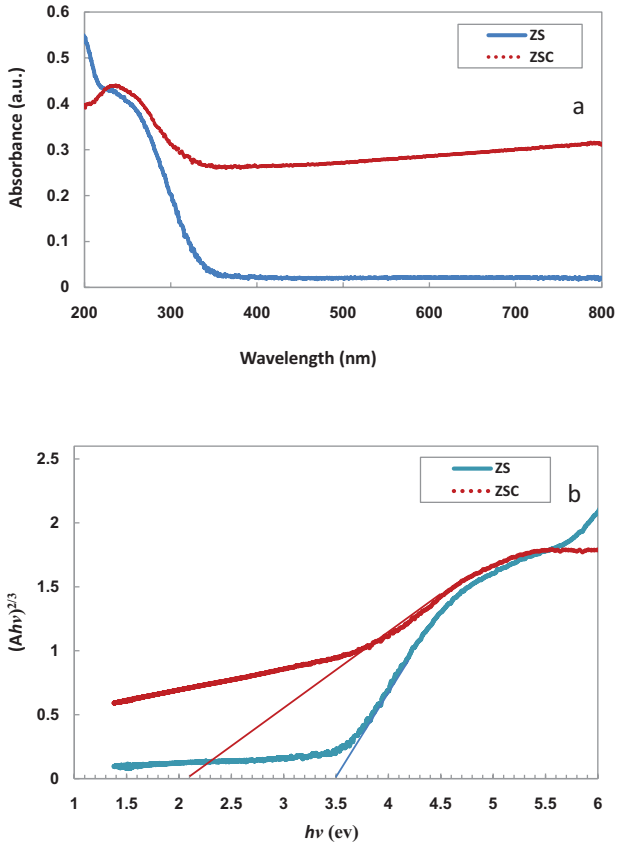

Fig. 4. (a) The UV–vis adsorption spectrum of synthesized ZS and ZSC, and (b) the corresponding TM plot of vs. energy of the photon.

$$(AE)^{1/m} = B(E - Eg) \quad (2)$$

In this equation, A represents the UV–vis absorbance, B is the proportional constant, and E is the photon energy (h). Moreover, the exponent m value refers to the type of electron transfer, which is the intrinsic property of the semiconductor.

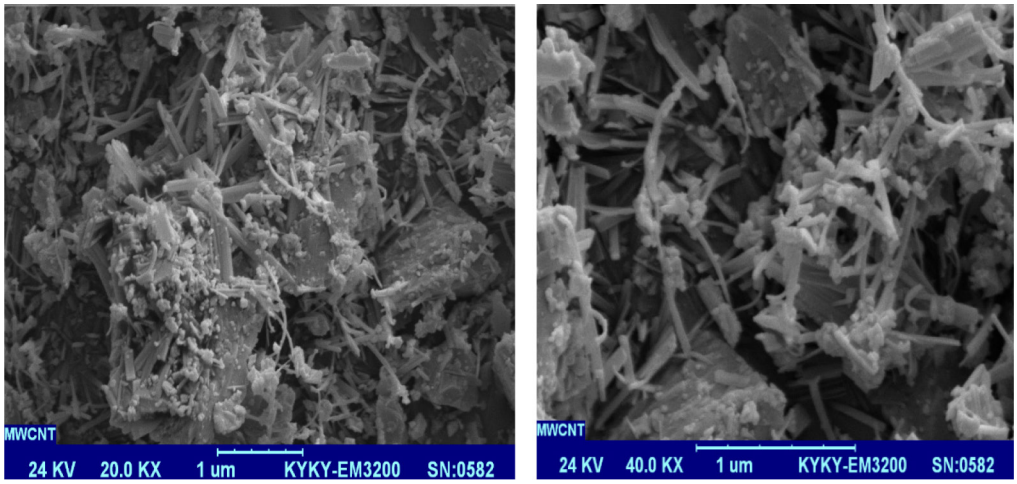

Fig. 3. SEM images of the prepared ZSC.

Its value equals 1/2, 3/2, 2, and 3 for direct allowed, direct forbidden, indirect allowed, and indirect forbidden transitions, respectively. This means that the type of transmission should be specified to assess the expansion demand from the DRS data. The band gap of ZS and ZSC was determined to be 3.5 and 2.1 eV, respectively, by extrapolating of the linear section of the TM plot to (Ahv) = 0 to intercept the hv axis.

4.2. The effect of operational parameters on dye removal process

The selected optimal values for the parameters were: photocatalyst dosage = 130 mg·L^{-1}, dye concentration = 10 mg·L^{-1}, pH = 9, and radiation source distance = 10 cm.

4.2.1. The effect of the initial concentration of dye

For this purpose, the experiments were performed with the initial dye concentration, varying from 10 to18 mg·L^{-1}, while the other parameters were kept under the optimal condition (Fig. 4a). The results showed that, at the low concentration, the removal efficiency increased. The phenomenon may be attributed to two main factors: 1) At the high dye concentration, the adsorbed dye molecules may have occupied all the active sites of the photocatalyst surface, thereby decreasing degradation efficiency. In the literature, it has also been reported that,at low concentrations, the ratio of available surface to initial pollutant concentration is larger, so the removal becomes independent of initial concentrations [27]; 2) another reason may be the absorption of the light photon by the dye itself, leading to a lesser availability of photons for hydroxyl radical generation [28]. Similar results have been reported in other studies. Nagarethamin et al. [29], for instance, reported that the percentage of removal decreases exponentially, while the amount adsorbed increased exponentially with the increase in the initial concentration of MB.

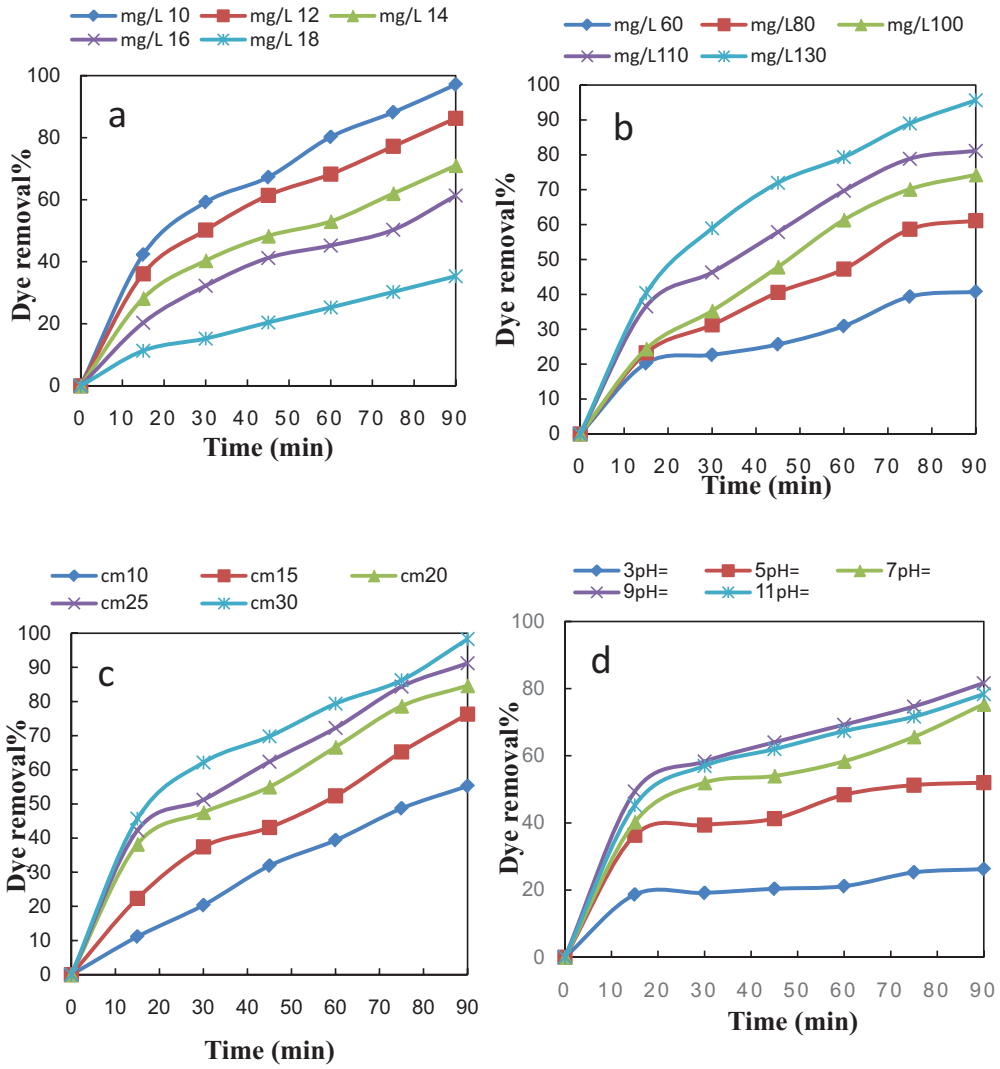

Fig. 5. The effect of the initial concentration of MB (a), photocatalyst dosage (b), distance from the source of radiation (c), and pH (d) on dye removal % in 90 min.

4.3. The effect of photocatalyst dosage

Fig. 4b illustrates the effect of photocatalyst dosage on MB removal efficiency. The results indicated that the removal efficiency increased with an increase in photocatalyst dosage. This observation can be explained in terms of the availability of active sites on the nanocomposite surface. Namely, the total active surface area increased with a decrease in photocatalyst dosage. The photocatalyst dosage of 130 mg·L^{-1} was selected as the optimal concentration. Similarly, Dorraji et al. [18] concluded that the increase in the removal rate of the dye with an enhancement of the quantity of catalyst can be attributed to the increased amount of surface area which creates a higher number of reactive sites for the photocatalytic reaction and adsorption of visible light by the photocatalyst. Increasing the surface area provides higher amounts of OH$^{\bullet}$ acting in favor of the photocatalytic removal of contaminant molecules [30–32].

4.4. The effect of solution surface distance from the source of radiation

To study the effect of solution surface distance from the source of radiation on removal efficiency, experiments were performed with distances varying from 10 to 30 cm while keeping the other parameters under optimal condition. Fig. 4c demonstrates that, by decreasing the distance, the intensity of the radiation (the number of photons) increased, and thus the removal efficiency increased. Masoumbeigi and Rezaee [33] reported that the intensity of radiation increased with a decrease in the distance between the source of radiation and the solution surface.

4.5. Effect of the initial pH

The effect of pH on the photocatalytic removal of MB was examined at different pH levels ranging from 3 to 11. Based on Fig. 4d, the amount of dye removal was remarkable in the alkaline medium. The reason for this trend depends on various factors such as the molecular structure of the dye. The dye is cationic, so no significant removal was observed in the acidic medium due to the electrostatic repulsion between dye and photocatalyst. At high pHs, i.e., pH = 11, due to the proliferation of OH$^-$ in the solution, the repulsion force between OH$^-$ and the photocatalyst surface occurred and the production of OH radicals decreased. The results of a similar study showed that, with increasing pH, dye removal increases [34].

4.6. Kinetics

In the heterogeneous photocatalytic oxidation, two steps can be considered for the process, the absorption step on the photocatalyst (Dye adherence was performed on the photocatalyst through the absorption process) and the photocatalytic reaction step. Therefore, the Langmuir-Hinshelwood model can be employed to describe the kinetics of photocatalytic oxidation processes. In this model, it is assumed that the reaction equation is the pseudo-first-order reaction to the pollutant:

$$-r_{dye\ \ removal} - \ln\left(\frac{C_t}{C_0}\right) = k_{app}t \tag{3}$$

where C_0 is the initial dye concentration, C_t is the dye concentration at time t, and k_{app} is the apparent first-order reaction rate. Fig. 5 depicts the plots of $-\ln(C_t/C_0)$ vs. t at various concentrations of the dye. On the basis of R^2 values (Table 1), the reaction rate of dye removal in each of the concentrations followed the first-order kinetics.

Also, k_{app} values decreased by increasing the concentration of the pollutant. This is due to the constant number of photocatalyst active sites against increasing concentrations of pollutant. The decrease in k_{app} values by increasing the initial concentration of the pollutant can be justified by the Langmuir-Hinshelwood model given below [17]:

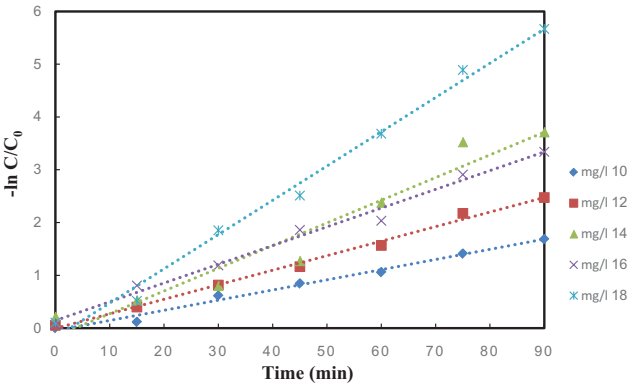

Fig. 6. The plots of $-\ln(C_t/C_0)$ vs. t.

Table 1
The rate constant of reaction at different concentrations

Dye	K_{app} (min^{-1})	R^2
mg/l10	0.9613	0.9999
mg/l12	0.6215	0.9996
mg/l14	0.3084	0.9736
mg/l16	0.1445	0.9251
mg/l18	0.0789	0.9532

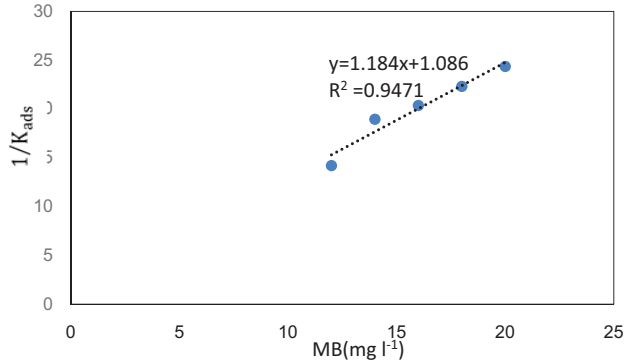

Fig. 7. The plots of $1/k_{app}$ vs. C_0.

$$-r_{dye\ removal} = k_c \frac{K_{ads}C_t}{1 + K_{ads}C_0} = k_{app}C_t \quad (4)$$

$$\frac{1}{k_{app}} = \frac{1}{k_c K_{ads}} + \frac{C_0}{k_c} \quad (5)$$

where k_c represents the rate constant of the surface reaction ($mg \cdot L^{-1} \cdot min^{-1}$) and K_{ads} denotes the equilibrium constant of adsorption ($L \cdot mg^{-1}$). By plotting $1/k_{app}$ vs. C_0, the values of K_{ads} and k_c can be calculated. Based on Fig. 6, the kinetics of the removal process followed the Langmuir-Hinshelwood model, and K_{ads} and k_c were obtained as 0.91 $L \cdot mg^{-1}$ and 0.84 $mg \cdot L^{-1} \cdot min^{-1}$, respectively.

5. Conclusion

The characterization techniques, namely XRD, FT-IR, and SEM confirmed the hydrothermally synthesized ZSC nanocomposite. The photocatalytic removal of dye in the presence of the prepared nanocomposite was influenced by several operational parameters such as the concentration of dye, photocatalyst dosage, pH, and distance from the source of radiation. The obtained optimal values of parameters for the removal of the dye were the following: photocatalyst dosage = 130 $mg \cdot L^{-1}$, dye concentration = 10 $mg \cdot L^{-1}$, pH = 9, and distance of the radiation source = 10 cm. The photocatalytic removal of dye was followed by pseudo-first-order and Langmuir-Hinshelwood kinetic models.

References

[1] M.H. Ehrampoush, M. Miri, S.M. Momtaz, M.T. Ghaneian, L. Rafati, H. Karimi, et al., Selecting the optimal process for the removal of reactive red 198 dye from textile wastewater using analytical hierarchy process (AHP), Desal. Water Treat., 56 (2016) 27237–27242.

[2] A.H. Gemeay, A.-F.M. Habib, M.A.B. El-Din, Kinetics and mechanism of the uncatalyzed and Ag (I)-catalyzed oxidative decolorization of Sunset Yellow and Ponceau 4R with peroxydisulphate, Dyes Pigm., 2 (2007) 458–463.

[3] M. Moradnia, M. Panahifard, K. Dindarlo, H.A. Jamali, Optimizing potassium ferrate for textile wastewater treatment by RSM, Environ. Health Eng. Manage. J., 3(3) (2016) 137–142.

[4] M. Montazerozohori, M. Nasr-Esfahani, Z. Moradi-Shammi, A. Malekhoseini, Photocatalytic decolorization of auramine and its kinetics study in the presence of two different sizes titanium dioxide nanoparticles at various buffer and non-buffer media, J. Ind. Eng. Chem., 21 (2015) 1044–1050.

[5] H. He, J. Huang, L. Cao, J. Wu, Photodegradation of methyl orange aqueous on $MnWO_4$ powder under different light resources and initial pH, Desalination, 252 (2010) 66–70.

[6] H. Nourmoradi, S. Zabihollahi, H. Pourzamani, Removal of a common textile dye, navy blue (NB), from aqueous solutions by combined process of coagulation–flocculation followed by adsorption, Desal. Water Treat., 57(11) (2016) 5200–5211.

[7] M. Moradnia, M.M. Emamjomeh, An environmental-friendly study on sanitary wastewater treatment for small community, Desal. Water Treat., 94 (2017) 25–30.

[8] D.J. Naghan, M.D. Motevalli, N. Mirzaei, A. Javid, H.R. Ghaffari, M. Ahmadpour, et al., Efficiency comparison of alum and ferric chloride coagulants in removal of dye and organic material from industrial wastewater-a case study, Bulgarian Chemical Communications. Specia, (2015) 206–210.

[9] P.A. Carneiro, G.A. Umbuzeiro, D.P. Oliveira, M.V.B. Zanoni, Assessment of water contamination caused by a mutagenic textile effluent/dyehouse effluent bearing disperse dyes, J. Hazard. Mater., 174 (2010) 694–699.

[10] R.O.A. de Lima, A.P. Bazo, D.M.F. Salvadori, C.M. Rech, D. de Palma Oliveira, G. de Aragão Umbuzeiro, Mutagenic and carcinogenic potential of a textile azo dye processing plant effluent that impacts a drinking water source, Mutat Res., 626 (2007) 53–60.

[11] M. Montazerozohori, S.A. Hoseinipour, Decolorization of p-dimethylaminobenzal-rhodanine under photocatalytic process by use of titanium dioxide nanoparticles at various buffer pHs, Environ. Eng. Manage. J., 16(9) (2017) 1853–1858.

[12] H. Javadian, M.T. Angaji, M. Naushad, Synthesis and characterization of polyaniline/γ-alumina nanocomposite: A comparative study for the adsorption of three different anionic dyes, J. Ind. Eng. Chem., 20(5) (2014) 3890–3900.

[13] G. Sharma, M. Naushad, A. Kumar, S. Rana, S. Sharma, A. Bhatnagar, F.J. Stadler, A.A. Ghfar, M.R. Khan, Efficient removal of coomassie brilliant blue R-250 dye using starch/poly (alginic acid-cl-acrylamide) nanohydrogel, Process Safe. Environ. Protect., 109 (2017) 301–310.

[14] C.-H. Wu, Effects of operational parameters on the decolorization of CI Reactive Red 198 in UV/TiO_2-based systems, Dyes Pigm., 77 (2008) 31–38.

[15] S. Taherkhani, M. Darvishmotavalli, B. Bina, K. Karimyan, A. Fallahi, H. Karimi, Dataset on photodegradation of tetracycline antibiotic with zinc stannate nanoflower in aqueous solution-Application of response surface methodology, Data Brief., 19 (2018) 1997–2007.

[16] K. Woan, G. Pyrgiotakis, W. Sigmund, Photocatalytic carbon-nanotube–TiO_2 composites, Adv. Mater., 21 (2009) 2233–2239.

[17] M. Montazerozohori, M. Nasr-Esfahani, S. Joohari, Photocatalytic degradation of an organic dye in some aqueous buffer solutions using nano titanium dioxide: a kinetic study, Environ. Protect. Eng., 38(3) (2012) 45–55.

[18] M.S. Dorraji, A. Amani-Ghadim, M. Rasoulifard, S. Taherkhani, H. Daneshvar, The role of carbon nanotube in zinc stannate photocatalytic performance improvement: experimental and kinetic evidences, Appl. Catal. B: Environ., 205 (2017) 559–568.

[19] B. Tan, E. Toman, Y. Li, Y. Wu, Zinc stannate (Zn_2SnO_4) dye-sensitized solar cells, J. Amer. Chem. Soc., 129(14) (2007) 4162–4163.

[20] C. Yan, J. Yang, Q. Xie, Z. Lu, B. Liu, C. Xie, S. Wu, Y. Zhang, Y. Guan, Novel nanoarchitectured Zn_2SnO_4 anchored on porous carbon as high performance anodes for lithium ion batteries, Mater. Lett., 138 (2015) 120–123.

[21] T. Peng, P. Zeng, D. Ke, X. Liu, X. Zhang, Hydrothermal preparation of multiwalled carbon nanotubes (MWCNTs)/CdS nanocomposite and its efficient photocatalytic hydrogen production under visible light irradiation, Energy Fuels., 25(5) (2011) 2203–2210.

[22] M.N. Sepehr, F. Allani, M. Zarrabi, M. Darvishmotevalli, Y. Vasseghian, S. Fadaei, M.M. Fazli, Dataset for adsorptive removal of tetracycline (TC) from aqueous solution via natural light weight expanded clay aggregate (LECA) and LECA coated with manganese oxide nanoparticles in the presence of H_2O_2, Data Brief, 22 (2018) 676–686.

[23] A.M. Baker, L. Wang, S.G. Advani, A.K. Prasad, Nafion membranes reinforced with magnetically controlled Fe_3O_4–MWCNTs for PEMFCs, J. Mate. Chem., 22 (2012) 14008–14012.

[24] Z.-Z. Jiang, Z.-B. Wang, Y.-Y. Chu, D.-M. Gu, G.-P. Yin, Carbon riveted microcapsule Pt/MWCNTs-TiO_2 catalyst prepared by in situ carbonized glucose with ultra high stability for proton exchange membrane fuel cell, Energy Environ. Sci., 4(7) (2011) 2558–2566.

[25] L. Shi, Y. Dai, Synthesis and photocatalytic activity of Zn_2SnO_4 nanotube arrays, J. Mater. Chem. A., 1 (2013) 12981–12986.

[26] M.A. Alpuche-Aviles, Y. Wu, Photoelectrochemical study of the band structure of Zn_2SnO_4 prepared by the hydrothermal method, J. Amer. Chem. Soc., 131(9) (2009) 3216–3224.

[27] Z.A. Al-Othman, R. Ali, M. Naushad, Hexavalent chromium removal from aqueous medium by activated carbon prepared from peanut shell: adsorption kinetics, equilibrium and thermodynamic studies, Chem. Eng. J., 184 (2012) 238–247.
[28] A. Khani, B. Pezeshki, Easy simultaneous synthesis–immobilization of nanosized CuO–ZnO on perlite as a photocatalyst for degradation of acid orange 7 from aqueous solution in the presence of visible light, Desal. Water Treat., 57(15) (2016) 7047–7053.
[29] N. Kannan, M.M. Sundaram, Kinetics and mechanism of removal of methylene blue by adsorption on various carbons—a comparative study, Dyes Pigm., 51 (2001) 25–40.
[30] K. Dashtian, M. Ghaedi, H. Shirinzadeh, S. Hajati, S. Shahbazi, Achieving enhanced blue-light-driven photocatalysis using nanosword-like VO_2/$CuWO_4$ type II n–n heterojunction, Chem. Eng. J., 339 (2018) 189–203.
[31] S. Mosleh, M. Rahimi, M. Ghaedi, K. Dashtian, S. Hajati, S. Wang, Ag_3PO_4/AgBr/Ag-HKUST-1-MOF composites as novel blue LED light active photocatalyst for enhanced degradation of ternary mixture of dyes in a rotating packed bed reactor, Chem. Eng. Process.: Process Intensif., 114 (2017) 24–38.
[32] S. Mosleh, M.R. Rahimi, M. Ghaedi, K. Dashtian, S. Hajati, Sonochemical-assisted synthesis of CuO/Cu_2O/Cu nanoparticles as efficient photocatalyst for simultaneous degradation of pollutant dyes in rotating packed bed reactor: LED illumination and central composite design optimization, Ultrason. Sonochem., 40A (2018) 601–610.
[33] H. Masoumbeigi, A. Rezaee, Removal of Methylene Blue (MB) dye from synthetic wastewater using UV/H_2O_3 advanced oxidation process, J. Health Policy Sustain. Health., 2(1) (2015) 160–166.
[34] P. Wang, M. Cao, C. Wang, Y. Ao, J. Hou, J. Qian, Kinetics and thermodynamics of adsorption of methylene blue by a magnetic graphene-carbon nanotube composite, Appl. Surface Sci., 290 (2014) 116–124.